Co_9S_8 as a Catalyst for Electroreduction of O_2: Quantum Chemistry Predictions

Reyimjan A. Sidik and Alfred B. Anderson*

Department of Chemistry, Case Western Reserve University, Cleveland, Ohio 44106

Received: August 10, 2005; In Final Form: November 8, 2005

The slab band quantum computational approach in the Vienna ab initio simulation package (VASP) is used to calculate the adsorption energies of reactants, reaction intermediates, and products in O_2 reduction and in water oxidation in acid on three crystallographic surfaces of pentlandite structure Co_9S_8. Reversible potentials for the reaction steps involving electron and proton transfer are determined by using the energies in a linear Gibbs free energy relationship. On the basis of these results, we find that the partially OH-covered (202) surface is active toward O_2 reduction and should have overpotential behavior similar to that observed for platinum electrodes. One structure in the predicted four-electron reduction mechanism is novel: S^{2-} provides an adsorption site for O following O−O bond scission, which, unlike the case of platinum electrodes, takes place prior to the first reduction step.

Introduction

In recent years, proton-exchange-membrane fuel cells (PEMFCs), regarded as potential replacements for internal combustion engines in transportation applications, are the subject of extensive research.[1,2] This is due to their high energy-conversion efficiency, low temperature of operation, and environmental benefits at the point of operation, particularly for hydrogen fuel. PEMFCs should also find other applications, such as generation of distributed electric power for commercial and residential markets and powering devices in the portable electronics market. There is a widespread ongoing effort to overcome three major challenges to commercialization of PEMFCs. These are lowering the cost and increasing the durability of the fuel cells and developing an infrastructure for distribution of the hydrogen fuel. The first two depend heavily on the properties of the electrocatalysts. Platinum and Pt alloys are used widely as catalysts for both anodes and cathodes because they have the best catalytic activities and chemical stabilities among the catalyst materials developed so far.[3] However, oxygen reduction at the cathode is not efficient enough, and this inefficiency accounts for most of the kinetic overvoltages in PEM fuel cells.[4] There is a strong incentive to find good alternative cathode electrocatalysts, preferably more active than Pt and less expensive. They must also be chemically stable.[1]

To this end, in the past three decades there has been a search for a replacement for platinum as the cathode material. A variety of nonnoble metal compounds have been studied including metal chelates,[5] activated carbon,[6] perovskites,[7] oxides,[8] and metal thiospinels.[9,10] The earliest non-Pt catalyst for oxygen reduction was reported by Jasinsky in 1964, who found cobalt phthalocyanine, a metallo-N_4 macrocycle, active for O_2 reduction in alkaline solution.[5] However, it was not stable in acidic medium. In the mid 1970s it was discovered that, by pyrolizing metallo N_4-macromolecules at 500−800 C° in an inert atmosphere, catalysts formed that were not only stable but also more active than they were prior to the heat treatement.[11] Efforts to identify the active sites with the hope of understanding the catalytic activities and stabilities are ongoing.[12]

* Corresponding author. E-mail: aba@case.edu; phone: 216-368-5044; fax: 216-368-3006.

In the past decade, transition-metal chalcogenides have been studied as O_2 reduction catalysts.[13−17] Alonso-Vante et al.[17] advanced the synthesis, electrochemical, and spectroscopic characterizations of these materials. The chalcogenides studied have been Mo−M−X and M−X, where M = Co, Ru, Re, or Rh and X = S, Se, or Te. Some of these compounds showed good activity toward O_2 reduction in acid.[18] Furthermore, the chalcogenide electrodes were, unlike platinum electrodes, resistant to poisoning by methanol crossing over from the anode side in direct methanol fuel cells.[17,19] Ex situ and in situ spectroscopic techniques were employed in attempts to determine the structures of the active sites of some of the best catalysts, such as $Mo_xRu_ySe_z$ and Ru_xX_y (X = S, Se, or Te).[20−22] Using the finding that the mean metal−metal nearest neighbor distances in Ru_xSe_y particles are nearly the same as those in pure Ru particles and that the particles are relatively stable in acid, Alonso-Vante et al. proposed that the Ru_xSe_y clusters contain cores composed of Ru atoms surrounded on the surface by both elements.[20,22] To account for the observed four-electron reduction of O_2 to water, it was proposed that O_2 adsorbs on twofold cation sites because such sites were believed to be needed for O−O bond cleavage.[20] However, the compositions and structures of the active sites on these catalysts are still not known. Although transition metal sulfides have been studied theoretically as hydrodesulfurization catalysts,[23,24] no theoretical studies have been reported concerning their catalytic activities in O_2 electroreduction.

This paper presents results of a theoretical analysis of three surfaces of Co_9S_8 for possible catalytic activity toward electroreduction of O_2. Calculated reversible potentials for the elementary reaction steps over several types of crystal surfaces are the basis for identifying catalytically promising surface structures. Co_9S_8 is selected because, among several transition metal sulfides, it was found to have the highest catalytic activity for O_2 reduction in acidic solution.[9,10]

Theoretical Method

A. VASP Calculations. The spin-polarized version of the Vienna ab initio simulation program (VASP) is employed.[25−29] This method uses a plane-wave basis and nonlocal Vanderbilt-

10.1021/jp054487f CCC: $33.50
Published on Web 12/18/2005

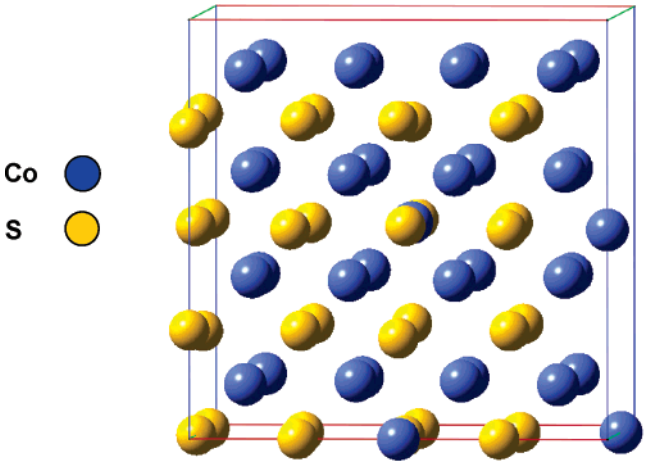

Figure 1. Conventional 68 atom cubic unit cell of Co_9S_8, with experimental cell constant $a = 9.9482$ Å.[35]

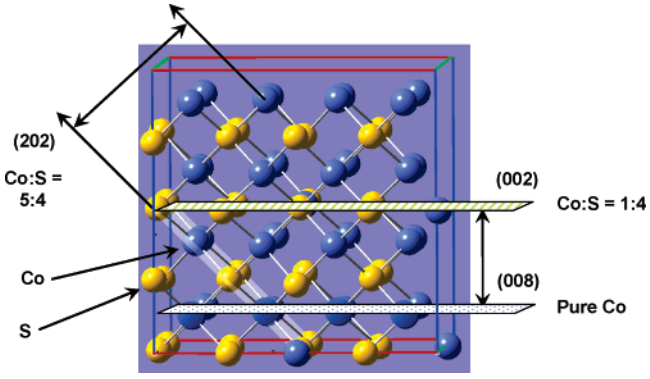

Figure 2. Cubic unit cell of Co_9S_8 with the optimized cell constant $a = 9.865$ Å. ($4Co_9S_8$, 68 atoms). Double arrows denote slabs studied in the calculations.

type ultra-soft pseudo potentials (US-PP) to describe the electron−ion interactions.[29] Exchange and correlation energies are approximated using functionals proposed by Perdew and Wang.[30] Self-consistent solutions of the Kohn−Sham equations for the electronic ground states are determined via an iterative unconstrained band-by-band matrix-diagonalization scheme that uses a residual minimization method.[28,31] The Brillouin zone integrations are performed with Monkhorst−Pack grids[32] and a generalized Gaussian smearing ($\sigma = 0.2$ eV) for the integrations in reciprocal space.[33] *k*-point convergence is established. A plane-wave energy cutoff is 400 eV because this cutoff was satisfactory for this type of calculation in prior work from this group.[30] Meshes of ($5 \times 5 \times 1$) *k* points are used for all of the calculations.

As in prior work,[34] surfaces are represented by slabs composed of four layers of substrate separated by 10 Å of vacuum. The conventional cubic unit cell[35] for pentlandite structure Co_9S_8 is in Figure 1, and the three surfaces studied and their slab models are defined in Figure 2. Adsorption on only one side of each of the slabs is considered. The two topmost layers and the adsorbates are relaxed, whereas the two deeper layers are frozen at the optimized unit cell geometry, as shown in Figure 3.

B. Model for Calculating Reversible Potentials for Forming Adsorbed Reaction Intermediates. The reversible potentials for the onset of water oxidation and for the elementary steps involved in O_2 reduction are calculated using a Gibbs linear free energy relationship.[34] The relationship is based on the idea of perturbing the intermediates, for which standard reversible potentials are known in bulk solution, by allowing them to bond to the catalyst. Some of the solvation bonds in the reactant and product are replaced by bonds to the catalyst, and these bond energies become useful parameters for defining the equilibrium condition for forming intermediates on the catalyst. Either experimental or calculated bond strengths may be used. An example, OH reduction in solution and on the Pt surface, is in eqs 1−4

$$U^\circ(\text{surface}) = U^\circ + (\text{product adsorption bond strength} - \text{reactant adsorption bond strength})/F \quad (1)$$

$$OH\cdot(g) + H^+(aq) + e^- \leftrightarrow H_2O(l) \quad U^o = 2.81 \text{ V (SHE)} \quad (2)$$

$$\downarrow -2.50 \text{ eV} \qquad \downarrow -0.42 \text{ eV}$$

$$Pt{-}OH + H^+(aq) + e^- \leftrightarrow Pt{-}OH_2 \quad (3)$$

$$U^\circ(\text{surface}) = 2.81 + 0.42 - 2.50 = 0.73 \text{ V (expt} \approx 0.55 \text{ V}, \theta \approx 0.0) \quad (4)$$

In eq 1, F is the Faraday constant and 2.81 V is the experimental reversible potential for OH reduction in acid solution.[36] The adsorption bond strengths for OH (2.50 eV) [37] and H_2O (0.42 eV)[38] are the low-coverage experimental values. Considering the uncertainties in the experimental bond strengths, the predicted 0.73 V water oxidation onset potential for Pt is reasonably close to the observed value of 0.55 V/SHE in acid in the absence of anion adsorption.[39]

C. Surface Models for the Co_9S_8 Electrocatalyst. This work examines three low Miller index surfaces of pentlandite structure Co_9S_8 in detail. From X-ray diffraction, the pentlandite space group is *Fm*3*m* (225) according to the compilation of Wyckoff,[35] with cell parameters given in Table 1. The unit cell shown in Figure 1 has a cubooctahedral structure with cell parameters $a = b = c = 9.9482$ Å. There are four Co_9S_8 units in the conventional cubic unit cell, with the sulfur atoms forming a nearly cubic close-packed framework. The unit cell has 2 types of cations, 4 in octahedral sites and 32 in tetrahedral sites. Among cobalt sulfide compounds CoS, CoS_2, Co_3S_4, and Co_9S_8, the pentlandite structure material is unique in having next-neighbor metal−metal bonds with interatomic distances equal to or less than that in Co metal: 2.333−2.486 Å for Co_9S_8 and 2.507 Å for Co metal. Earlier band calculations have shown that Co_9S_8 has nearly the same density of states function near the Fermi level as cobalt metal.[24] This is consistent with the ability of the sulfide to conduct electron current.

The theoretically optimized bulk cell constant, using VASP, is 9.8650 Å, which is in satisfactory agreement with the experimental value of 9.9284 Å. On the basis of crystallographic planes, many different surface compositions are possible for the cubooctahedral pentlandite structure. Three surfaces of diverse composition are selected: (008), which is terminated with cobalt, (002), which is sulfur rich (Co:S = 1:4), and (202), which is a mixed surface (Co:S = 5:4). These surface planes and the four-layer slabs used for the surface modeling are defined in Figure 2. The bottom face of the four-layer (008) surface is the (002) surface. Four-layer slabs were found satisfactory in prior studies using VASP for calculating reversible potentials for water oxidation and O_2 adsorption on Pt and its alloys.[34,40]

In the absence of adsorbates, the calculated atom relaxations in the top two layers are small, as shown in Figure 3. The stability gains per $2Co_9S_8$ upon relaxation are 0.346, 0.268, and 0.646 eV for the (008), (002), and (202) surfaces, respectively.

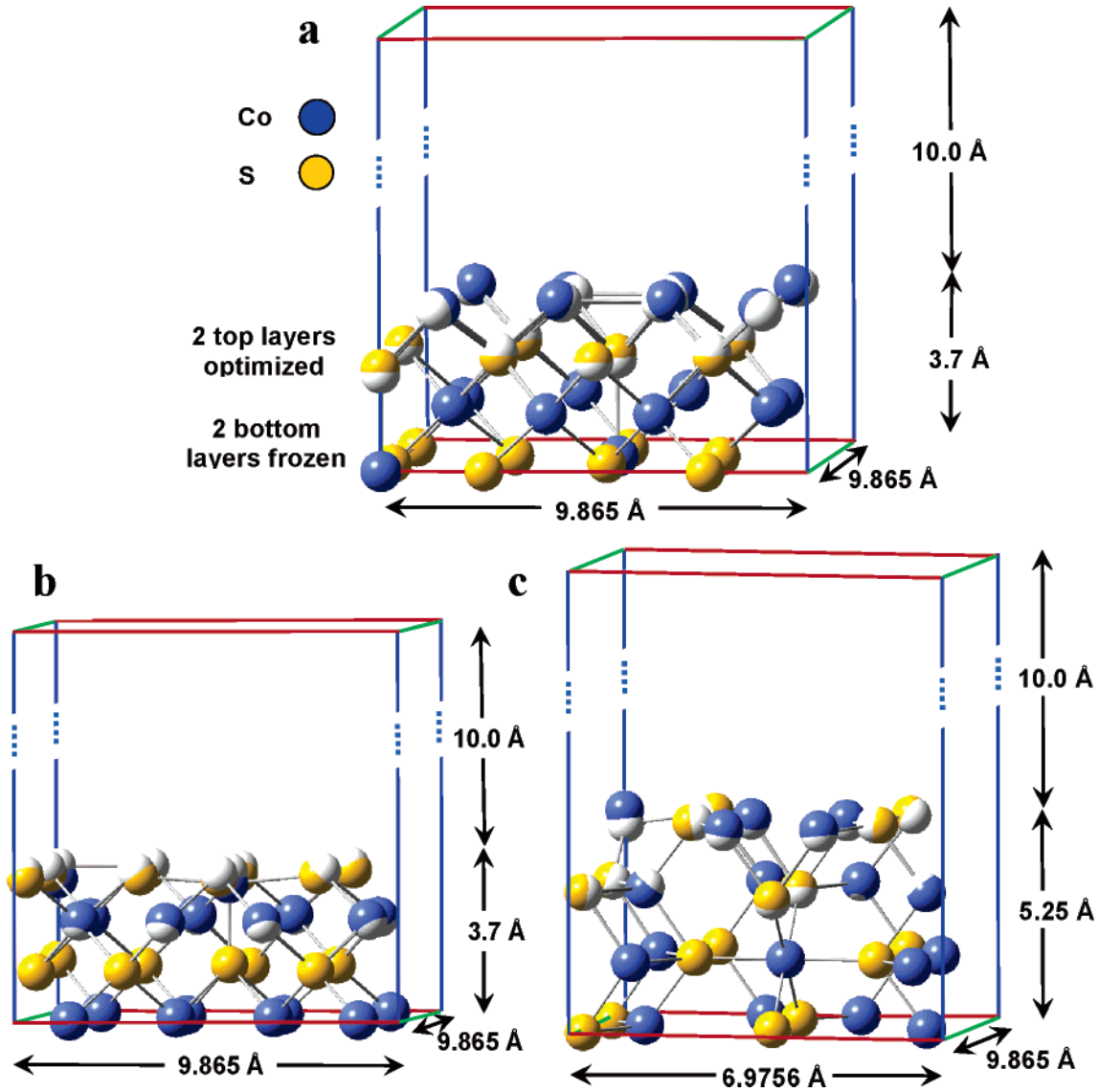

Figure 3. Side view of atom relaxations constrained to the top two layers; (a) (008), (b) (002), (c) (202). The white balls are the optimized positions of atoms relaxed from their calculated bulk positions. These overlap the colored balls, which represent the bulk positions.

TABLE 1: Atom Coordination and Positions in Pentlandite Structure Co_9S_8[a]

atom	position	*X*	*Y*	*Z*
Co(t)	(4b)	0.5000	0.5000	0.5000
Co(o)	(32f)	0.1260	0.1260	0.1260
S	(8c)	0.2500	0.2500	0.2500
S	(24e)	0.2591	0.0000	0.0000

[a] Wyckoff notation: Co(t), tetrahedral sites; Co(o), octahedral sites; space group, *Fm*3*m*(225).[35]

The total energy from VASP for the bulk unit cell is the same with and without spin-polarization, indicating that the bulk material is nonmagnetic. For the four-layer slabs allowance for spin polarization results in up to 1.0 eV stabilization, so calculations for all surfaces employed spin-polarization.

Results

A. Adsorption of H_2O and O_2. Water is a product of the O_2 reduction reaction, but in low-tempreature PEM fuel cells, excess water is needed during O_2 reduction as an aid to proton transfer. The OH(ads) reduction equilibrium in eq 3 is believed to control the overpotential at the Pt cathode because OH(ads) blocks surface sites against O_2 adsorption.[40−44] For cobalt sulfide, OH(ads) may also be expected to play a role. Whether water molecules might bond strongly to surface sites and block O_2 adsorption must be considered because it is a reduction product that must be removed from the catalytic site.

Calculated coverage-dependent adsorption energies for H_2O, OH, and O_2 on various sites of the three Co_9S_8 surfaces are given in Table 2, and the optimized structure for water adsorption on the (202) surface is shown in Figure 4a. The low-coverage water adsorption bond strength of 0.640 eV on the (008) surface is similar to that on Pt, but the 3.289 eV OH adsorption energy is much greater, so at low coverage OH(ads) should form from H_2O at potentials greater than 0.16 V. O_2 adsorbs strongly and dissociatively on the clean surface. Might increased OH(ads) coverage passivate the surface to further water oxidation, leaving some sites available for O_2 adsorption? At higher OH(ads) coverages the adsorption bond strengths remain high, between 3.23 and 3.55 eV. Therefore, the (008) surface is predicted to be OH(ads)-covered and inactive for oxygen reduction in the potential range of interest.

The sulfur-rich (002) surface has widely separated Co atoms. The calculations indicate that it has the right properties for two-electron O_2 reduction. The H_2O and O_2 adsorption energies are very close to those for Pt, and the OH adsorption bond is weaker

TABLE 2: Low-Coverage Values for Adsorption Bond Strengths (eV) for H_2O, OH, and O_2 on Three Surfaces of Co_9S_8 and the Resulting Predicted Water Oxidation Potentials, $U°$(V)

surface Miller index	adsorption bond strength			H_2O oxidation potential
	H_2O	OH	O_2	
(008) pure Co	0.640[a]	3.289[a]	2.486[b]	0.16
(002) S-rich	0.448[c]	2.217[c]	0.552 end-on, 0.070 side-on[c]	1.04
(202) mixed	0.375[d]	3.880[d]	1.054 end-on, 1.995 bridge[d]	0.35
	1.692[e]	3.863[e]		0.64
	0.580[f]	1.751[f]		1.64

[a] For one adsorbate per eight surface Co sites. [b] For dissociative adsorption. [c] For one adsorbate per two widely separated Co sites. [d] For coverage as in Figure 4b. [e] For second H_2O and OH as in Figure 5. [f] For third H_2O and OH as in Figure 5.

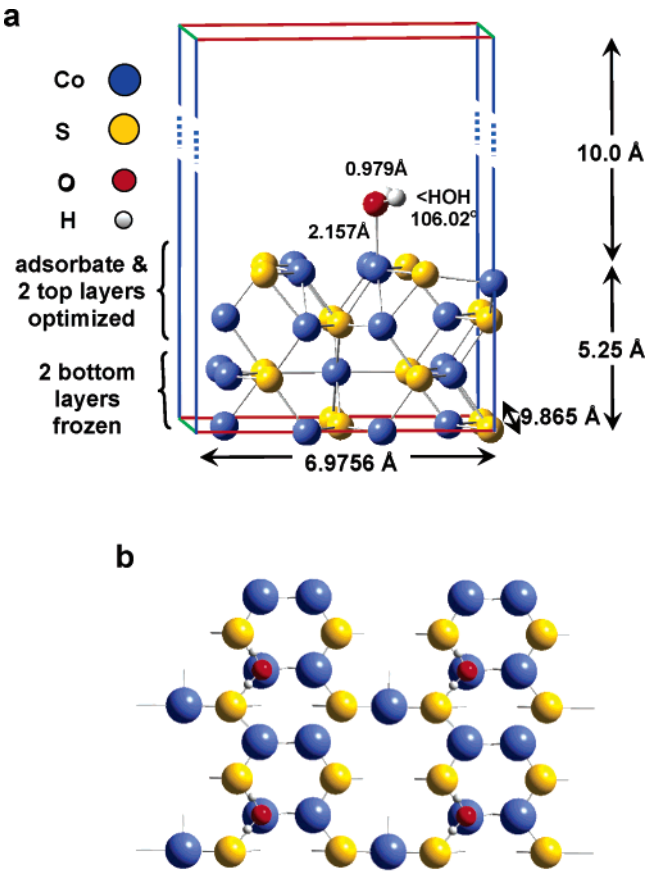

Figure 4. Side (a) and top (b) views for H_2O adsorption on onefold Co sites on the mixed (202) surface. Only the top layer for four translational cells is shown in b. The Co−O bond is perpendicular to the surface.

than that for Pt. This results in an H_2O oxidation potential of 1.04 V, which is positive of that for Pt. However, the end-on adsorption orientation for O_2 on the isolated Co sites on this surface is more stable (Table 2). This should lead to peroxide formation, and it precludes four-electron reduction to water. Therefore, the (002) surface is a proposed candidate for the observed peroxide generation on Co_9S_8.[10]

The (202) mixed surface has a metal−sulfur ratio of 5:4 and consists of multiple metal atom sites that are believed to be needed for the four-electron reduction. As may be seen in Table 2, O_2 bonds molecularly in both end-on atop and bridge orientations on this surface. However, the water oxidation potential at the atop site is 0.35 V at low coverage (Figure 4b), an unfavorably low value, and OH bonding to a twofold site

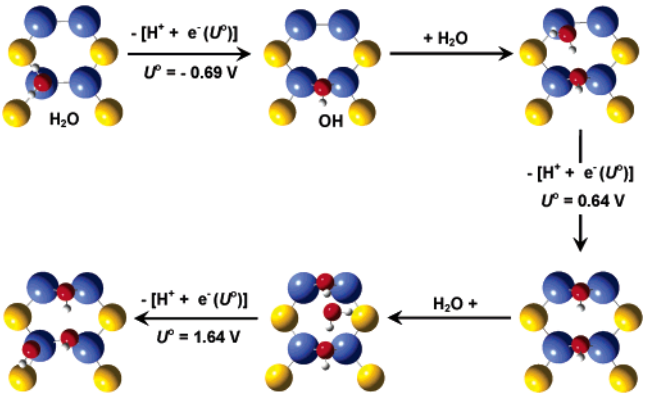

Figure 5. Top view of water oxidation steps to form an OH(ads) passivated (202) surface of Co_9S_8.

between adjacent Co atoms is stronger, resulting in an even less favorable −0.69 V reversible potential for OH(ads) formation there, as shown in Figure 5. A water molecule added to an adjacent Co pair has reversible potential for oxidation of 0.64 V when the OH(ads) product is in the bridge site. The fourfold Co site now has two bridging OH(ads). A third H_2O forms hydrogen bonds to the two OH(ads) and is oxidized at 1.64 V to OH(ads) in a onefold site. Because the H_2O molecule does not bond stably directly on the adsorption site, one could use the value of zero eV, as was done in a recent study of oxygen reduction on Cu^I sites in a model of copper laccase,[45] and in this case, the reversible potential becomes 1.06 eV. Both are consistent with this partially OH(ads) covered surface being a candidate for the oxygen electrode. A summary of these results is in Figure 5. The next section shows that this surface has the right properties for four-electron O_2 reduction at reasonably low overpotential.

B. O_2 Reduction on the Hydroxylated (202) Surface. As is evident from the optimized geometry of the partially OH-covered surface in Figure 6, there could be enough space for O_2 molecules to adsorb onto the rectangular open spaces formed by the four Co atoms. Calculations indicate that this can happen. O_2 adsorbs dissociatively onto these sites: one O atom stays near the center, coordinated to four metal atoms, and the other bonds to the neighboring sulfur, as shown in Figure 7. The dissociative adsorption is exothermic by 1.13 eV and has no barrier. Predicting S^{2-} as an adsorption site for O is an interesting aspect of this reaction, made possible by the ability of S to be stable in the +4 oxidation state.

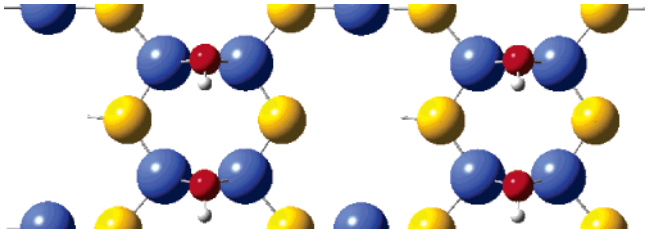

Figure 6. Top view of the partially OH(ads)-covered (202) surface that is the proposed active surface for four-electron oxygen reduction.

The goal here is to find high reversible potential pathways for the four-electron reduction. The difference between the lowest reversible potential along a pathway and 1.229 V largely determines overpotential for the pathway. The pathway with the lowest overpotential for the overall four-electron reduction is sought. There are two possibilities for the first reduction step: reduction of the central O bonded to four Co first or reduction of O bonded to S first, followed by the reduction of

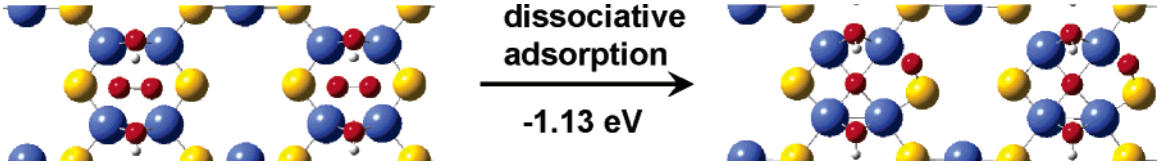

Figure 7. Top view of (a) the initial approach of O_2 and (b) the dissociation products on the partially OH(ads)-covered (202) surface of Co_9S_8.

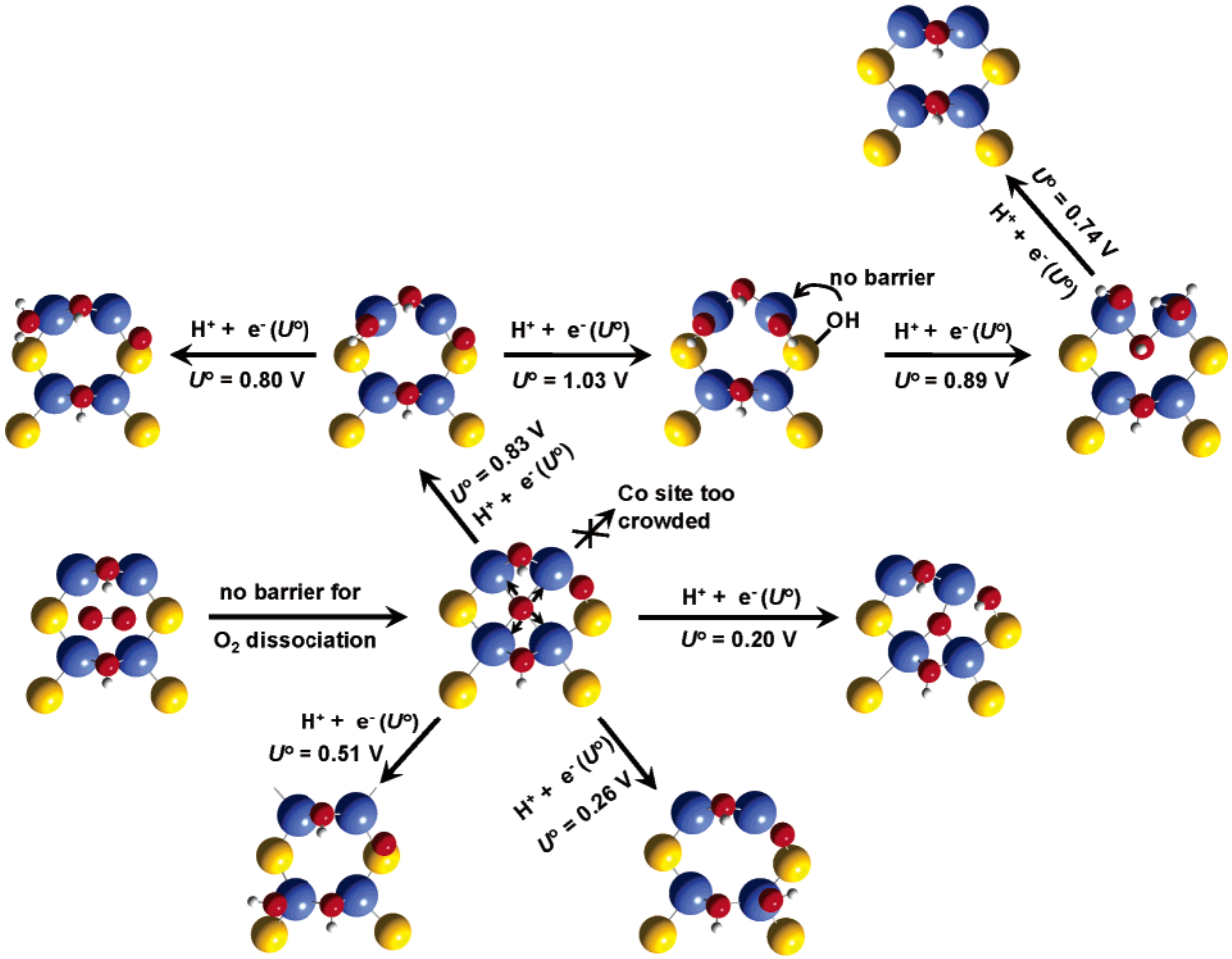

Figure 8. Top view of reduction pathways examined for the adsorbed O atoms on the partially OH(ads)-covered (202) surface of Co_9S_8.

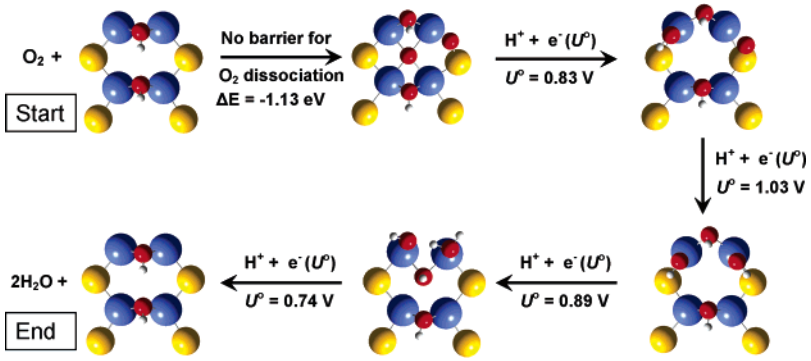

Figure 9. Top view of the reduction cycle for O_2 on the partially OH(ads)-covered (202) surface of Co_9S_8.

the other O. According to Figure 8, five sites may be available for the OH(ads) formed from reducing the O bonded to the fourfold Co site first, but the Co atom at the upper right corner of the rectangle is eliminated because of crowding. O−S reduction occurs at 0.20 V and reduction of the central O occurs at a maximum potential of 0.83 V, making this the better first reduction step. The second high-potential step is reduction of the O atom on sulfur at 0.89 V. This OH moves without a barrier to the neighboring Co site. The other pathways for the first two reduction steps, shown in Figure 9, are less favorable.

The predicted steps of the O_2 reduction cycle on the partially OH-covered (202) surface are in Figure 9. Following the first reduction at 0.83 V, the O on sulfur is reduced spontaneously to OH(ads) because its reversible potential is higher, 1.03 V. After reduction of these two O atoms, the sequential reductions

of the product adsorbed OH groups to water occur at relatively favorable potentials of 0.89 and 0.74 V, respectively. These final two steps complete the cycle by regenerating the initial hydroxylated surface. The 0.74 V step determines the overpotential for the overall four-electron reduction, suggesting an activity similar to platinum for this surface. The 1.13 eV heat loss accompanying the dissociative adsorption of O_2 is the cause of the low potentials for the O(ads) and OH(ads) reduction steps. An even better catalyst will be one to which O_2 bonds and dissociates with less released heat.

Conclusions

On the basis of the adsorption bond strengths of the reactants, reaction intermediates, and products for water oxidation and O_2 reduction, the partially OH-covered (202) surface of Co_9S_8 should be active toward O_2 reduction. Water molecules do not block the active sites on this surface. The heat loss from O_2 dissociative chemisorption necessitates overpotential for the four-electron process. The effect of the free energy dissipation spreads among all of the intermediates because the result is that the Co−O and Co−OH bonds are stronger than optimal.

Another result of this study is the prediction of O bonding to S, a nonmetallic surface site. Quantum chemical modeling work suggested already in one instance that adsorption intermediates could bond to a nonmetal site, but in that case hydrogen peroxide was stabilized by hydrogen bonding to an N lone pair on an $Fe-N_4$ system.[46] It is concluded that O_2 reduction overpotential on the (202) surface of Co_9S_8 is similar to that for platinum electrodes. This study does not establish whether the surface is structurally robust or stable but implies that experimental characterization of the surfaces of Co_9S_8 oxygen cathodes would be worthwhile.

Acknowledgment. This work was supported by the Department of Energy through a subcontract from the University of South Carolina and by a Multi-University Research-Initiative (MURI) Grant DAAD19-03-1-0169 from the Army Research Office to Case Western Reserve University.

References and Notes

(1) http://www.eere.energy.gov/hydrogenandfuelcells/fuelcells/, Oct. 2005.
(2) *Handbook of Fuel Cells: Fundamentals, Technology, Applications*, four-volume set; Vielstich, W., Lamm A., Gasteiger H., Eds.; John Wiley & Sons: New York, 2003.
(3) Markovic, N. M.; Ross, P. N. *Surf. Sci. Rep.* **2002**, *45*, 117.
(4) Adzic, R. Recent Advances in the Kinetics of Oxygen Reduction. In *Electrocatalysis*; Lipkowski, J., Ross, P. N., Eds.; Wiley-VCH: New York, 1998; p 197.
(5) Jasinsky, R. *Nature (London)* **1964**, *201*, 1212.
(6) Morcos, I.; Yeager, E. *Electrochim. Acta* **1970**, *15*, 953.
(7) Tsueng, A. C. C.; Bevan, H. *J. Electroanal. Chem.* **1973**, *45*, 429.
(8) King, W. J.; Tsueng, A. C. C. *Electrochim. Acta* **1974**, *19*, 485.
(9) Baresel, D.; Sarholz, W.; Scharner, P.; Schmitz, J. *Ber. Bunsen-Ges.* **1974**, *78*, 608.
(10) Behret, H.; Binder, H.; Sandstede, G. *Electrochim. Acta* **1975**, *20*, 111.
(11) Bagotzky, V. S.; Tarasevich M. R.; Radyushkina K. A.; Levina O. E.; Andrusyova S. I. *J. Power Sources* **1977**, *2*, 233.
(12) Dodelet J. P. In *N_4-Macrocyclic Metal Complexes: Electrocatalysis, Electrophotochemistry & Biomimetic Electroanalysis*; Zagal, J., Bedioui, F., Dodelet, J. P., Eds.; Springer: New York, 2006; Chapter 3.
(13) Alonso-Vante, N.; Tributisch, H. *Nature (London)* **1986**, *323*, 431.
(14) Alonso-Vante, N.; Schubert, B.; Tributisch, H.; Perrin, A. *J. Catal.* **1988**, *112*, 384.
(15) Trapp, V.; Christensen, P.; Hamnett, A. *J. Chem. Soc., Faraday Trans.* **1996**, *92*, 4311.
(16) Reeve, R. W.; Christensen, P. A.; Hamnett, A.; Haydock, S. A.; Roy, S. C. *J. Electrochem. Soc.* **1998**, *145*, 3463
(17) Alonso-Vante, N. References in the following review: Novel Nanostructured Materials Based on Transition Metal Compounds for Electrocatalysis. In *Catalysis of Nanoparticles Surfaces*; Wieckowski, A., Savinova, E., Vayenas, C., Eds.; Marcel Dekker: New York, 2003; p 931.
(18) Alonso-Vante, N.; Tributsch, H.; Solorza-Feria, O. *Electrochim. Acta* **1995**, *40*, 567.
(19) Shukla, A. K.; Raman, R. K. *Annu. Rev. Mater. Res.* **2003**, *33*, 155, and references therein.
(20) Malakhov, I. V.; Nikitenko, S. G.; Savinova, E. R.; Kochubey, D. I.; Alonso-Vante, N. *J. Phys. Chem. B* **2002**, *106*, 1670.
(21) Dassenoy, F.; Vogel, W. Alonso-Vante, N. *J. Phys. Chem. B* **2002**, *106*, 12152.
(22) Alonso-Vante, N.; Malakhov, I. V.; Nikitenko, S. G.; Savinova, E. R.; Kochubey, D. I. *Electrochim. Acta* **2002**, *47*, 3807.
(23) Raybaud, P.; Kresse, G.; Hafner, J.; Toulhoat, H. *J. Phys.: Condens. Matter*. **1997**, *9*, 11107.
(24) Raybaud, P.; Kresse, G.; Hafner, J.; Toulhoat, H. *J. Phys.: Condens. Matter*. **1997**, *9*, 11085.
(25) Kresse, G.; Furthmuller, J. *Phys. Rev. B* **1996**, *54*, 11169.
(26) Kresse, G.; Hafner, J. *Phys. Rev. B* **1993**, *47*, 558.
(27) Kresse, G.; Hafner, J. *Phys. Rev. B* **1994**, *49*, 14251.
(28) Kresse, G.; Furthmuller, J. *Comput. Mater. Sci.* **1996**, *6*, 15.
(29) Kresse, G.; Hafner, J. *J. Phys.: Condens. Matter*. **1994**, *6*, 8245.
(30) Perdew, J. P.; Wang, Y. *Phys. Rev. B* **1992**, *45*, 13244.
(31) Wood, D. M.; Zunger, A. *J. Phys. A* **1985**, *18*, 1343.
(32) Monkhorst, H. J.; Pack J. D. *Phys. Rev. B* **1976**, *13*, 5188.
(33) Methfessel, M.; Paxton A. T. *Phys. Rev. B* **1989**, *40*, 3616.
(34) Anderson, A. B.; Roques, J. *J. Electrochem. Soc.* **2004**, *151*, E85.
(35) Wyckoff, R. W. G. *Crystal Structures*; John Wiley & Sons: New York, 1964; Vol. 2, p 222.
(36) Anderson, A. B.; Albu, T. V. *J. Electrochem. Soc.* **2000**, *147*, 4229.
(37) Mooney, C. E.; Anderson, L. C.; Lunsford, J. H. *J. Phys. Chem.* **1993**, *97*, 2505.
(38) Sexton, B. A.; Hughes, A. E. *Surf. Sci.* **1984**, *140*, 227.
(39) Markovic, N. M.; Adzic, R. R.; Cahan, B. D.; Yeager, E. B. *J. Electroanal. Chem.* **1994**, *377*, 249.
(40) Roques, J.; Anderson, A. B. *J. Electroanal. Chem.* **2004**, *151*, E340-E347.
(41) Anderson, A. B.; Roques, J.; Mukerjee, S.; Murthi, V. S.; Markovic, N. M.; Stamenkovic, V. *J. Phys. Chem. B* **2005**, *109*, 1198−1203
(42) Mukerjee, S.; Srinivasan, S.; Soriaga, M. P.; McBreen, J. *J. Electrochem. Soc.* **1995**, *142*, 1409.
(43) Markovic, N. M.; Schmidt, T. J.; Grgur, B. N.; Gasteiger, H. A.; Behm, R. J.; Ross, P. N. *J. Phys. Chem. B* **1999**, *103*, 8568.
(44) Stamenkovic, V.; Schmidt, T. J.; Ross, P. N.; Markovic, N. M. *J. Phys. Chem. B* **2002**, *106*, 11970.
(45) Schweiger, H.; Vayner, E.; Anderson, A. B. *J. Electrochem. Solid State Lett*. **2005**, *8*, A585.
(46) Anderson, A. B.; Sidik, R. A. *J. Phys. Chem. B* **2004**, *108*, 5031.